

Numerical simulation of touchdown dynamics of thermal-flying-height-control sliders

Jinglin Zheng and David B. Bogy

Computer Mechanics Laboratory

Department of Mechanical Engineering

University of California at Berkeley

Abstract

With the advent of thermal-flying-height-control (TFC) technology, the physical spacing in magnetic hard disk drives is now reduced to sub-1nm. At this limit, tribological flyability and reliability become critical issues for the performance of the read-write head. In this paper, a numerical approach is applied to study the touchdown dynamics of TFC sliders, by expanding a 3-degree-of-freedom slider dynamics model to a 250-degree-of-freedom head-gimbal assembly dynamics model and considering several significant tribological effects at this ultra-low clearance (adhesion, tribo-charge, friction, contact, etc.). The simulation results show that the slider's vibration amplitude increases substantially at the beginning of touchdown, and it gets suppressed with further reduction in flying height. Analysis in the frequency domain shows the excitation of the second air bearing pitch mode when instability occurs. The expansion of the dynamic system to include a realistic model of the suspension is shown to be important in determining the frequency of the excited mode. Adhesion force is shown to play an essential role in exciting the second air bearing pitch mode and causing instability, while electrostatic force and friction force affect only the slider's dynamics at instability. Friction force is also shown to be related to the excitation of the first air bearing mode.

Keywords: Thermal flying-height control, head-gimbal assembly, head-disk interface, interfacial forces

1. Introduction

The physical clearance between the read-write head and disk in magnetic recording hard disk drives (HDD) has been continuously decreasing in the past decades in order to meet the ever-increasing demand for higher areal density of stored data. In recent years, thermal flying-height control (TFC) technology has been widely used to achieve an ultra-low physical clearance at the read-write transducers. The local area around the read-write transducers is heated during reading or writing operations by use of a heating element imbedded in the air bearing slider body, resulting in a bulge at the transducer area. The clearance at the transducer location is thus reduced by several nanometers while other parts of the slider stay well above the disk [1-6]. With the application of TFC technology current air bearing sliders can fly at a clearance of $\sim 1\text{nm}$ where the slider is subject to increasing interactions with the disk and thus experiences a much more complicated dynamics.

Touchdown dynamics of TFC sliders has received much attention because it is concerned with the flying-height limit of flying sliders, and it is also related to the feasibility of a contact recording slider [7-9]. Experiments have shown that TFC sliders often experience relatively large bouncing vibrations at air bearing frequencies when the power supplied to the heating element is increased beyond a critical point, which is usually termed the “touchdown” power. Such vibrations can get damped out when the slider is over-pushed by even higher heating power [10-12]. Considering the complicated nature of the head-disk interface, a numerical tool that is capable of capturing the slider’s characteristic dynamics can be very helpful for exploring the mechanisms behind these phenomena as well as facilitating design improvements.

In this paper a numerical tool is provided for simulating a TFC slider’s touchdown process. A time-varying heater-induced protrusion profile is used to reduce the slider’s flying height and induce touchdown. A full finite element model of a head-gimbal assembly is reduced to a 250-degree-of-freedom (250-DOF) mass-spring system, and the dynamics equation of this system is solved at each time step. Simulation results show similar trends at touchdown as compared with experimental findings. The inclusion of the suspension dynamics in the numerical

model is shown to be important for determining the frequencies of the excited vibration modes during touchdown. Also, different HDI forces (adhesion, friction, electrostatic) are shown to contribute in quite different ways to the slider's dynamics at touchdown.

2. Numerical model

A numerical approach based on the CML dynamics solver is developed for conducting the touchdown analysis. The generalized Reynolds equation is solved using a finite volume approach to obtain the lift force arising from the airflow between the slider and disk [13]. In previous approaches, the suspension was modeled as a massless spring with three degrees of freedom in the FH, pitch and roll directions [14]. However, recent experiments have shown that the suspension can have substantial vibrations during touchdown that interact significantly with the air bearing slider. Therefore, in this study, we expand the simplified model in [14] by using finite element (FE) modeling and reduction techniques for the suspension. A three dimensional FE suspension model with a femto-sized slider attached is reduced to a 250-DOF mass-spring system using ANSYS substructuring analysis and a CML reduction program [15]. Even with the reduction vibration modes up to 150kHz are retained from the original model and the relative error of frequencies is found to be within 10% of the results from modal analysis on the full FE model. In this way, the original 3-DOF dynamic system is expanded to a 250-DOF dynamic system, the dynamics of which is solved at each time step so that the suspension-slider interactions can be captured throughout the simulation.

A sub-boundary lubrication model is implemented in this dynamic solver to model the interfacial forces (contact, adhesion, friction, electrostatic) arising at the HDI at extremely small clearances [16-17]. These forces are calculated based on a multi-asperity approach: the surface is assumed to have asperities with an areal density, uniform radius of curvature, and statistically distributed heights. Forces occurring at a single asperity with a specific asperity height at a certain clearance are calculated and then integrated over the range of asperity heights, in order to obtain the force acting on one asperity at this clearance. Interfacial forces are calculated at each

grid point and integrated over the entire air bearing surface. The roughness parameters are taken from [18], which are based on atomic force microscopy images of slider and disk surfaces. Usage of the multi-asperity approach also allows solving for the air bearing pressure at zero or negative FH's that can occur at contact regions. Thus, the air bearing pressure loss due to contact is also accounted for in the current numerical scheme.

To bring the slider from a flying state to touchdown we use a time-varying actuation profile as the input to modify the air bearing geometry at each time step. Here we use the protrusion geometry from [19] as a base geometry. According to the peak protrusion value specified in the actuation profile we modify this protrusion geometry proportionally. An LDV (Laser Doppler Vibrometer) measured disk profile is used to simulate the moving waviness on the disk [20].

3. Results and discussions

3.1 Typical touchdown dynamics

As shown in Figure 1, a ramping-up actuation signal ranging from 18nm to 30nm is applied to actuate the slider from flying to touchdown, and the flying-height modulation at the read transducer location is plotted as a function of time. The vibration amplitude of the slider shows a non-monotonic trend: it starts increasing rapidly at about 1.2ms, remains high between 1.5ms and 2ms, and then gets suppressed under further protrusion. Here, we designate the actuation range where the slider's vibration amplitude becomes obviously larger as the instability region.

To show the slider's contact status with the disk during this process, we plotted the history of the contact force in Figure 2. The contact force remains at zero at the beginning time steps and then it becomes non-zero at around 1.2ms. If we consider the occurrence of a positive contact force as the sign of touchdown and compare Figure 2 with Figure 1 we conclude that the instability occurs at the beginning of touchdown. Between 1.2ms and 2.5ms the contact force oscillates between positive values and zero, which means that the slider comes into contact and then bounces off the disk. Throughout the instability region the slider's motion is characterized by this intermittent slider-disk contact. Beyond 2.5ms, the contact force is always above zero,

indicating that the slider is continuously sliding on the disk. We also see that the slider's vibration amplitude at this stage is relatively small.

To examine the slider's dynamics in the frequency domain we conducted Fourier transforms of the data points over every 0.2ms band, assuming that the slider's dynamics does not change abruptly within this time interval. The power FFT of the transducer's FH is shown in Figure 3 as a color map varying with actuation and frequency. An obvious red stripe indicating high amplitude is observed at around 280kHz when the actuation steps are between 20.5nm and 24nm. This stripe corresponds to the strong dynamics observed in the time domain (Figure 1) and the length of the stripe corresponds to the extent of the instability region. Higher harmonics of this excited mode are also observed at ~560kHz. It is worth noting that similar frequency peaks have been discovered in touchdown experiments and reported in [11]

Figure 4 shows the power FFT results for the transducer's FH at 4 actuation steps: 21nm, 22nm, 23nm, and 24nm. A small peak first appears at 249kHz at 21nm actuation, then it moves to 283kHz at the 22nm actuation with a much higher amplitude. The peak frequency then increases further to 298kHz with the peak height substantially reduced at 23nm actuation. At 24nm, the peak frequency is even higher and the amplitude is further reduced.

The method elaborated in [14] is employed here to identify the nodal line in correspondence with each peak observed from Figure 4. As shown in Figure 5, all nodal lines are located near the slider's leading edge, thus the excited mode is considered to be the second air bearing pitch mode. With increasing actuation, the nodal line moves more toward the trailing edge and the frequency becomes higher. The increase in frequency with higher actuation is considered to be an effect of further compression of the air film at the trailing edge. In addition, assuming the pitch torque applied by the suspension remains essentially constant, to maintain the force balance of the slider, the nodal line has to move toward the trailing edge as the pressure at the trailing edge grows with increasing protrusion.

3.2 Effect of suspension mass and stiffness

In the current numerical model the FE model of the suspension with a rigid slider attached is reduced to a 250-DOF mass-spring system using the method described in [15], and the dynamics of this system is solved at each time step. In this way, the interaction between the suspension and slider can be captured while keeping the problem solvable within a reasonable amount of time. To show the effect of including the suspension mass and stiffness we first simplify the procedure used in section 3.1 by modeling the suspension as a spring with simple stiffnesses in the FH, pitch and roll directions, and we repeat the simulation presented in section 3.1 by applying the same actuation profile. The transducer's FH history obtained with this simplified procedure is shown in Figure 6, and it is compared with the results obtained in section 3.1 in Figure 7. An instability region can still be identified for the simpler case; however, the vibration amplitude at instability as well as the extent of the instability region are different.

The power FFT of the transducer's FH as a function of the actuation and its frequency is obtained by repeating the same procedure as outlined in section 3.1 and shown in Figure 8. Referring to Figures 3 and 8, one observes in both the 3-DOF and 250-DOF cases, a red stripe indicating strong vibrations at certain actuation ranges exists, however, the vibration frequency for the 3-DOF case is $\sim 370\text{kHz}$, much higher than the 250-DOF case, which is $\sim 280\text{kHz}$. The nodal line for the excited mode of 366.2kHz at about 21nm actuation is shown in Figure 8. The location of the nodal line confirms that the excited mode is still the second air bearing pitch mode, although the frequency has increased substantially. Thus, the suspension is actively involved in the air bearing slider vibrations, resulting in a much reduced frequency of the second air bearing mode in the 250-DOF case. Furthermore, when we push the slider beyond the instability region, the second air bearing frequency is further raised due to the growing pressure peak at the slider's trailing edge. It goes up to $\sim 500\text{kHz}$ for the 250-DOF case, much less than $\sim 700\text{kHz}$ for the 3-DOF case, a frequency much higher than what has been discovered in experiments. Therefore, the inclusion of suspension-slider dynamic coupling is very important for determining the active vibration modes at touchdown and correlating them with experimental results.

3.2 Effects of interfacial forces

The effect of each interfacial force on the slider's touchdown dynamics is investigated using a simplified approach: we set just one of the interfacial forces to zero and then conduct the simulation again by applying the same actuation signal; the results are then compared with the case shown in 3.1 which includes all interfacial forces. The object is to find out how the slider's dynamics differs with or without that force. Three interfacial forces are studied using this approach: adhesion, electrostatic and friction forces.

3.2.1 Adhesion force

The first set of results is obtained by setting the adhesion force equal to zero. In Figure 9, we compare the transducer's FH with increasing protrusions obtained with and without adhesion force. One major difference is that the instability region disappears when adhesion force is taken out of the simulation. The vibration amplitude of the slider does not experience any obvious changes throughout the touchdown process for this case. In addition, the FH at the transducer location is slightly higher when the adhesion force is excluded, due to the reduced attractive effect in this case. The power FFT result shown in Figure 10 further confirms that no obviously excited modes can be observed when the adhesion force is excluded. This result indicates that adhesion force plays an essential role in inducing the touchdown instability.

3.2.2 Electrostatic force

Figure 11 shows the transducer's FH varying with protrusion when the electrical potential difference between the slider and disk is set to zero so that the electrostatic force equals zero in this case. For comparison, the same curve obtained in section 3.1 is also shown in Figure 11. An obvious instability region exists in both cases, although the extent of the instability region and the vibration amplitude at instability are different in the two cases. Due to the attractive nature of the electrostatic force, at the same actuation, the slider flies at a larger FH when the electrostatic force is excluded, thus touchdown occurs at a higher actuation value for this case, and so does the instability.

The power FFT of the transducer's FH for the electrostatic-force-excluded case is shown in Figure 12, where a red stripe is seen at around $\sim 300\text{kHz}$. The frequency is slightly higher compared with the case shown in section 3.1, because taking out the electrostatic effect stiffens the head-disk interface. The instability region starts at about 22nm and extends beyond 26nm , which is obviously wider than the electrostatic-force-included case (Figure 3). The power FFT results for 4 actuation steps (23nm , 24nm , 25nm and 26nm) presented in Figure 13 show a similar trend in the variation of the excited air bearing mode: the frequency increases monotonically while the amplitude first increases then decreases. It is interesting to note that although the electrostatic force and adhesion force are both attractive, they have different and distinct effects on the slider's dynamics: adhesion force is essential in causing instability and exciting the second air bearing pitch mode, while electrostatic force does not determine whether or not instability occurs. Such a difference is attributed to the fact that electrostatic force does not increase as rapidly with spacing reduction as adhesion force at sub- 1nm clearances. Also, compared with the electrostatic force, adhesion force is mostly concentrated at the trailing edge, and thus it is more likely to excite the second air bearing mode. In addition, because of the expanded instability region and increased amplitude at the second air bearing mode in the electrostatic-force-excluded case, we conclude that the electrostatic force serves to suppress the slider's dynamics at the second air bearing mode in the studied case.

3.2.3 Friction force

Figure 14 shows plots of the transducer's FH as a function of protrusion when the friction force is turned off in the simulation, and the curve is compared with the one obtained in section 3.1. Similar to the electrostatic force case, eliminating the friction force does not eliminate the instability region. However, the slider actually has a stronger dynamics at the instability region and such instability continues for a wider actuation range. The result in the frequency domain is shown in Figure 15 where we observe a longer red stripe at $\sim 250\text{kHz}$. The power FFT's at 21nm , 22nm , 23nm , 24nm and 25nm are shown in Figure 16, and they show that the nature of the touchdown dynamics does not change: the second air bearing mode gets excited from

a certain actuation step and gets suppressed as the slider goes through even higher actuation. A major difference is that the excited second air bearing mode is stronger and is damped out more slowly, which shows that friction force also suppresses the unstable dynamics at the second air bearing mode. Another observation is that a mode gets excited at around 146.5kHz, as can be seen from the light red stripe in Figure 15, as well as the small peak in Figure 16. As shown by the nodal line at the slider's trailing edge (plotted in Figure 16), this peak is related to the first air bearing mode. This observation implies that the friction force makes contributions to the first air bearing mode, and in this case it suppresses its excitation.

4. Conclusion

A numerical approach is provided and used to study the touchdown dynamics of TFC sliders. An actuation signal ramping up with time is applied to bring the slider from flying to touchdown. The slider's flying-height modulation shows that an instability region exists at the beginning of touchdown, where the slider bounces on the disk at the second air bearing frequency. This instability disappears as the slider is brought into even closer contact with the disk with higher actuation.

By simplifying the suspension model to that of a massless, 3-D spring, we found that suspension mass and stiffness play important roles in determining the frequency of the excited second air bearing mode and correlating simulation results with experiments.

By taking one interfacial force out at a time, we found that each interfacial force plays a different role in affecting the slider's touchdown dynamics. Adhesion force is essential for causing touchdown instability and exciting the second air bearing mode, while electrostatic force and friction force only have minor effects in the slider's pattern of motion at instability. In this case study, both electrostatic force and friction force suppress the excited air bearing mode and enhance the ending of instability, and friction force also suppresses the first air bearing mode.

References

[1] Suk, M., Miyake, K., Kurita, M., Tanaka, H., Saegusa, S., and Robertson, N.: Verification of thermally induced nanometer actuation of magnetic recording

transducer to overcome mechanical and magnetic spacing challenges. *IEEE Trans. Magn.* 41, 4350-4352 (2005)

[2] Kurita M., Shiramatsu T., Miyake K., Kato A., Soga M., Tanka H., Saegusa S. and Suk M.: Active flying-height control slider using MEMS thermal actuator. *Microsyst. Technol.* 12, 369-375 (2006)

[3] Juang JY, Bogy D. B. and Bhatia C. S.: Alternate air bearing slider designs for areal density of 1 Tbit/inch². *IEEE Trans. Magn.* 42, 241-246 (2007)

[4] Juang JY and Bogy D. B.: Air-bearing effects on actuated thermal pole-tip protrusion for hard disk drives. *ASME J. Tribol* 129, 570 -578 (2007)

[5] Juang JY, Nakamura T., Knigge B., Luo Y. S., Hsiao W. C., Kuroki K., Huang F. Y. and Baumgart P.: Numerical and experimental analyses of nanometer-scale flying height control of magnetic head with heating element. *IEEE Trans. Magn.* 44, 3679-3682 (2008)

[6] Liu N., Zheng J. and Bogy D. B.: Predicting the flying performance of thermal flying-height control sliders in hard disk drives. *J. Appl. Phys.* 108, 016102 (2010)

[7] Li N., Zheng L., Meng Y., and Bogy D. B.: Experimental study of head-disk interface flyability and durability at sub-1nm clearance, *IEEE Trans. Magn.* 45, 3624-3627 (2009)

[8] Su L., Hu Y., Lam E. L., Li P., Ng R. W., Liang D., Zheng O., Liu H., Deng Z., and Zhang J.: Tribological and Dynamic Study of Head Disk Interface at Sub-1-nm Clearance. *IEEE Trans. Magn.* 47, 111-116 (2011)

[9] Vakis, A. I., Lee, S. C., and Polycarpou, A.: Dynamic head-disk interface instabilities with friction for light contact (surfing) recording. *IEEE Trans. Magn.*, 45, 4966-4971 (2009)

[10] Canchi S. V. and Bogy D. B.: Slider Dynamics in the Lubricant-Contact Regime. *IEEE Trans. Magn.* 46, 764-769 (2010)

[11] Zeng Q., Yang CH, Ka S., and Cha E.: An Experimental and Simulation Study of Touchdown Dynamics. *IEEE Trans. Magn.* 47, 3433-3436 (2011)

[12] Sheng G. and Xu J.: A parameter identification method for thermal flying-height control sliders. *Microsyst. Technol.* 17, 1409-1415 (2011)

- [13] Hu, Y.: Head-disk-suspension dynamics. Ph.D. thesis, University of California, Berkeley (1996)
- [14] Zheng, J and Bogy D. B.: Dynamic instability of thermal-flying-height-control sliders at touchdown. 21th ASME Annual Conference on Information Storage and Processing systems (2011)
- [15] Gupta, V.: Air bearing slider dynamics and stability in hard disk drives. Ph.D. thesis, University of California, Berkeley (2007)
- [16] Stanly, H. M., Etsion, I., and Bogy, D. B.: Adhesion of contacting rough surfaces in the presence of sub-boundary lubrication. ASME J. Tribol. 112, 98–104 (1990)
- [17] Zheng, J. and Bogy, D. B.: Investigation of flying height stability of thermal fly-height control sliders in lubricant or solid disk contact with roughness. Tribol. Lett., 38, 283–289 (2010)
- [18] Chen D. and Bogy D. B.: Intermolecular force and surface roughness models for air bearing simulations for sub-5 nm flying height sliders. Microsyst. Technol. 13, 1211-1217 (2006)
- [19] Zheng, J., Bogy, D. B., Zhang S. and Yan W.: Effects of altitude on the thermal flying height actuation. Tribol. Lett., 40, 295-299 (2010)
- [20] Chen D. and Bogy D. B.: Six-DOF vibrations of partial contact sliders in hard disk drives. Microsyst. Technol. 10-11, 1539-1546 (2007)

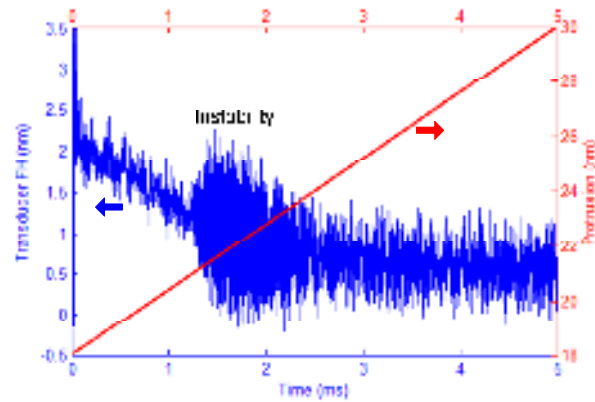


Figure 1 Heater induced protrusion (red) and transducer's FH (blue) as functions of time. An instability region where the slider experiences stronger vibrations exists at a certain protrusion range.

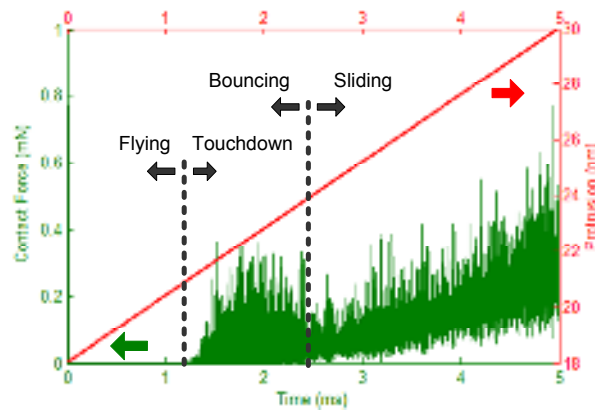


Figure 2 Heater induced protrusion (red) and contact force (green) as functions of time. Three regions (flying, bouncing and sliding) can be identified from the contact force history curve. The slider's motion at instability is characterized by strong bouncing vibrations.

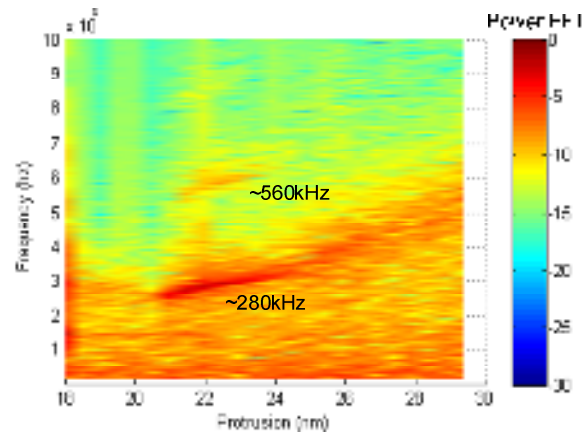


Figure 3 Power FFT of the transducer's FH as a colormap of frequency and protrusion. A mode at ~ 280 kHz with higher harmonics is excited at instability.

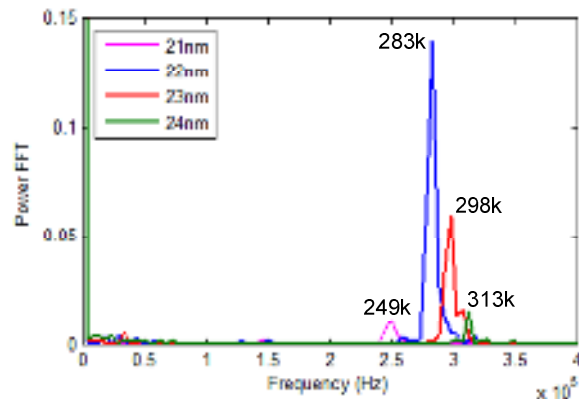


Figure 4 Power FFT of the transducer's FH at 4 actuation steps: 21 nm, 22 nm, 23 nm and 24 nm. The frequency of the excited mode keeps increasing while the amplitude first increases, then decreases.

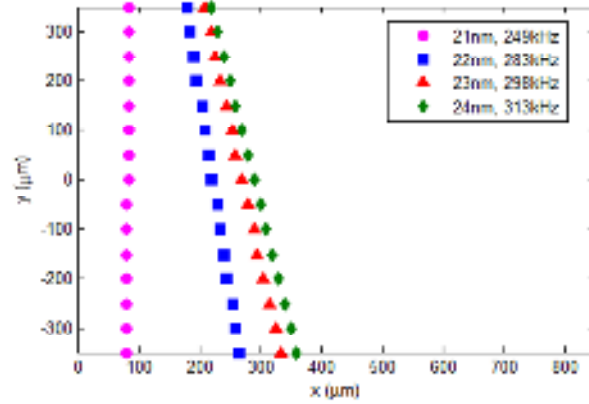


Figure 5 Nodal lines of the excited modes observed from Figure 4. These modes are getting excited as the slider goes through the instability region. All nodal lines are located near the leading edge of the slider.

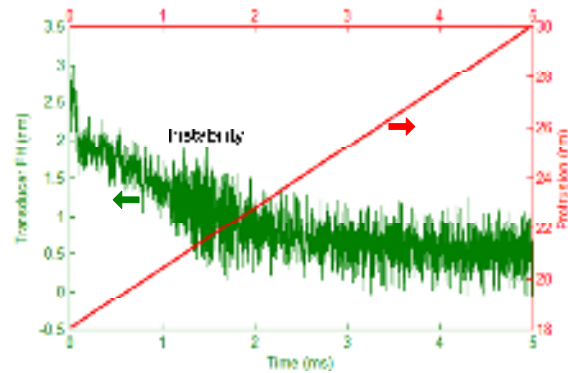


Figure 6 Heater induced protrusion (red) and transducer's FH (green) as functions of time. The head-disk-assembly is modeled as a 3-DOF mass-spring system where suspension is a massless 3-DOF spring. Instability still exists in this case.

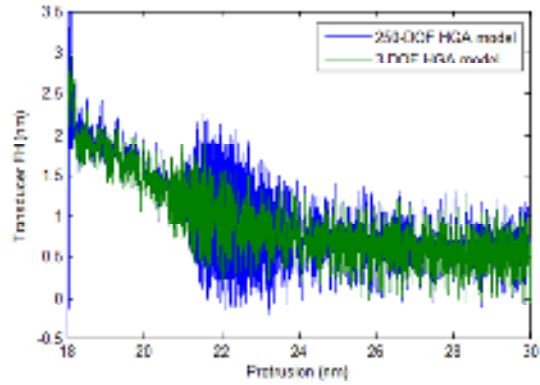


Figure 7 Comparing transducer's FH's as functions of protrusion when HGA is models as a 250-DOF (blue) and 3-DOF (green) mass-spring system. Both cases have instabilities, but the extent of the instability region and the vibration amplitude at the instability region differ.

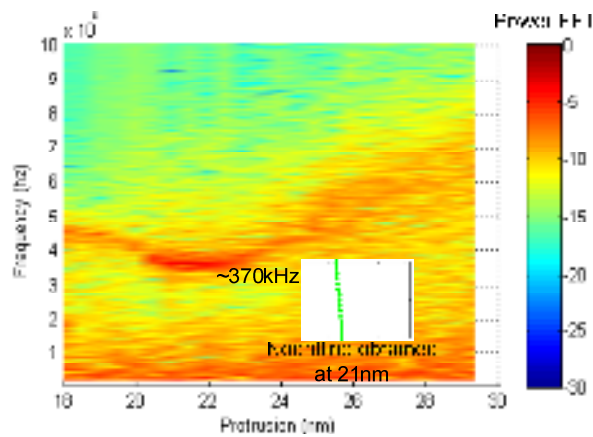


Figure 8 Power FFT of transducer's FH as a colormap of frequency and protrusion for the 3-DOF case. A mode at ~370kHz is excited at instability, the nodal line of which is located near the leading edge of the slider.

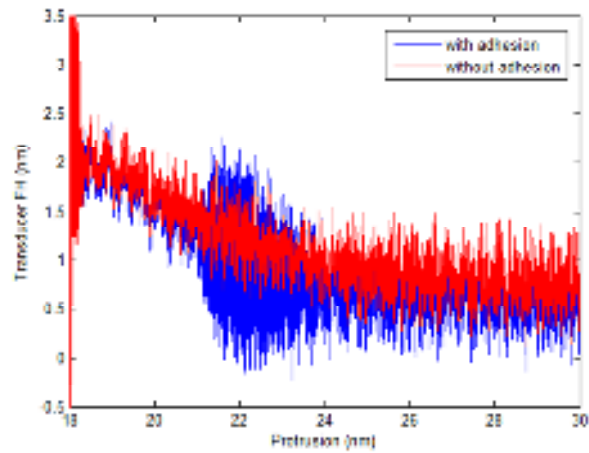


Figure 9 Comparing transducer's FH's as functions of protrusion when adhesion is included in (blue) or excluded from (red) the simulation. Instability only occurs in the adhesion-included case.

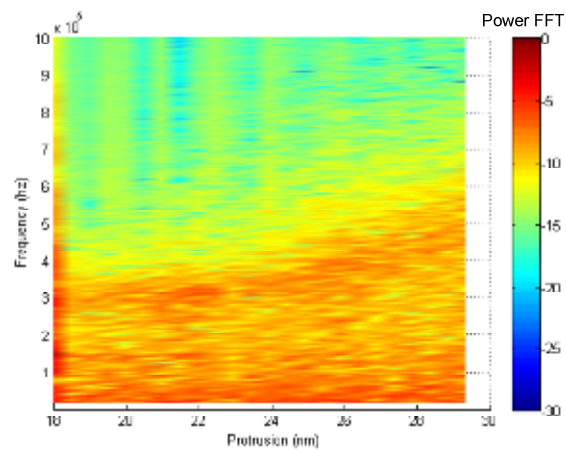


Figure 10 Power FFT of transducer's FH as a colormap of frequency and protrusion for the adhesion-excluded case. No obviously excited modes are observed during touchdown.

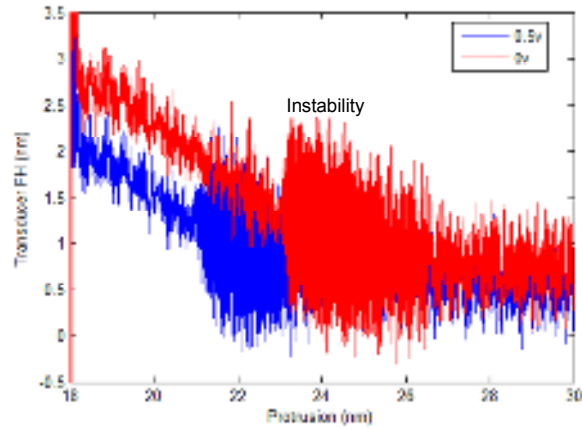


Figure 11 Comparing transducer's FH's as functions of protrusion when electrostatic force is included (blue) or excluded (red). Both cases have instabilities, but the extent of the instability region and the vibration amplitude at the instability region differ.

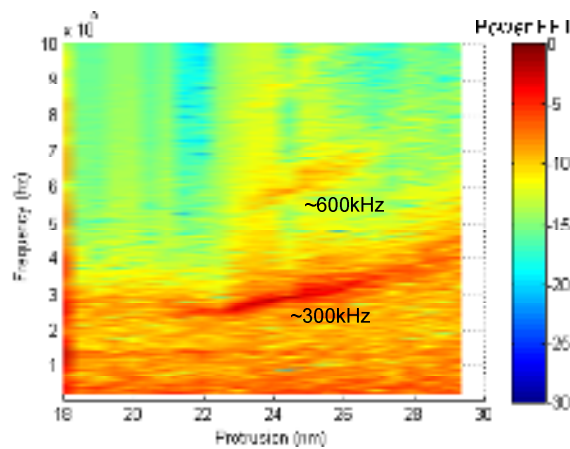


Figure 12 Power FFT of transducer's FH as a colormap of frequency and protrusion for the electrostatic-force-excluded case. A mode at $\sim 300\text{kHz}$ and its higher harmonics are excited at instability.

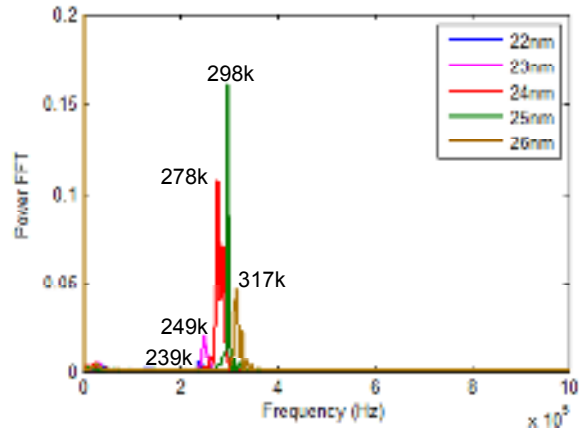


Figure 13 Power FFT of transducer's FH at 5 actuation steps: 22nm, 23nm, 24nm, 25nm and 26nm, for the electrostatic-force-excluded case. Similar to the electrostatic-force-included case (Figure 4), the frequency of the excited mode keeps increasing while the amplitude first increases, then decreases.

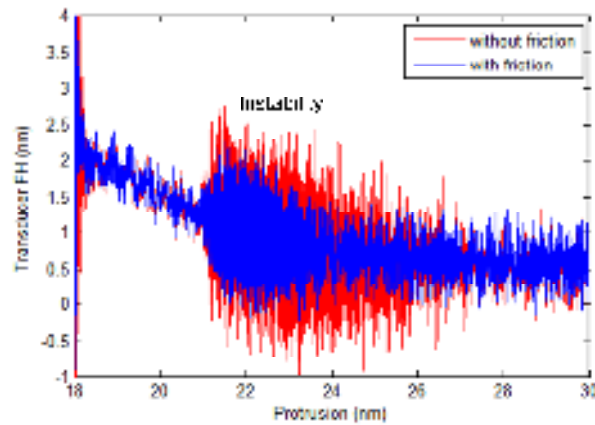


Figure 14 Comparing transducer's FH's as functions of protrusion when friction force is included (blue) or excluded (red). Both cases have instabilities, but the extent of the instability region and the vibration amplitude at the instability region differ.

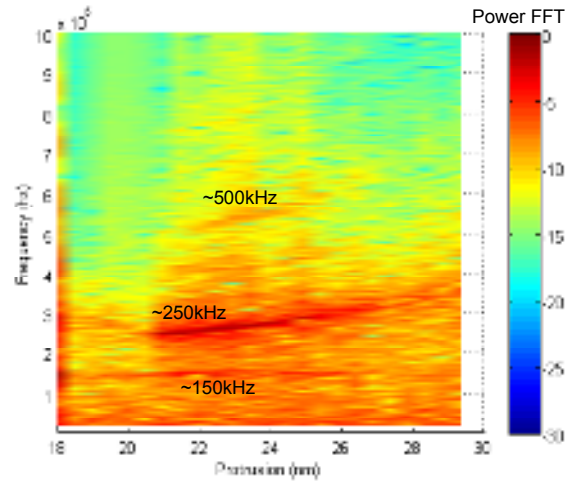


Figure 15 Power FFT of transducer's FH as a colormap of frequency and protrusion for the electrostatic-force-excluded case. A mode at ~250kHz and its higher harmonics are excited at instability. A mode at ~150kHz is also excited.

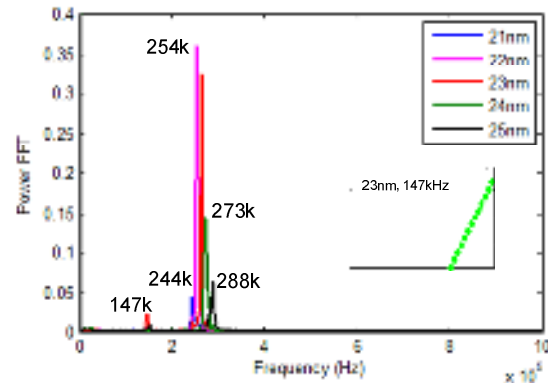


Figure 16 Power FFT of transducer's FH at 5 actuation steps: 21nm, 22nm, 23nm, 24nm and 25nm, for the friction-excluded case. Similar to the friction-included case (Figure 4), the frequency of the excited second air bearing mode keeps increasing while the amplitude first increases, then decreases. A 147kHz mode with a nodal line located at the slider's trailing edge is also excited.